Asian Journal of Chemistry; Vol. 30, No. 6 (2018), 1374-1382

ASIAN JOURNAL OF CHEMISTRY

https://doi.org/10.14233/ajchem.2018.21262

Efficiency Enhancement of Flexible Dye Sensitized Solar Cell Using TiO_2 Nanotube/ZnS Nanoparticles Photoanode

GHAIDA SALMAN MUHAMMED[1,*], MANAL MEDHAT ABDULLAH[1] and ABDULKAREEM MOHAMMED ALI AL-SAMMARRAIE[2]

[1]Department of Physics, College of Science, University of Baghdad, Baghdad, Iraq
[2]Department of Chemistry, College of Science, University of Baghdad, Baghdad, Iraq

*Corresponding author: E-mail: ghaidasalman7@gmail.com

Received: 30 January 2018; *Accepted*: 30 March 2018; *Published online*: 30 April 2018; AJC-18897

A composite material, TiO_2 nanotube arrays/ZnS nanoparticles (TNT/ZnS NPs) was assembled by deposition of ZnS nanoparticles onto anodized TiO_2 nanotube by sequential chemical bath deposition method. The tube-based photoanodes are crystallized at 550 ºC prior to solar cell construction. The effect of annealing of TiO_2 nanotube films at 550 ºC and pH values (7.5, 8.5 9.5) of prepared ZnS nanoparticles on the photovoltaic performance of flexible solar cells is studied. The characteristics of the flexible dye-sensitized solar cell were examined using a polyaniline as a counter electrode and KI/I_2 as an electrolyte. Ruthenium dye (N719) was used as an active layer. The characterizations of the films were also accomplished by using atomic force microscopy, scanning electron microscopy, energy dispersive X-ray spectroscopy, X-ray diffractometry and FTIR. The flexible dye-sensitized solar cells of TNT/ZnS nanoparticles photoanode achieved a power conversion efficiency of 0.75 % under 80 mW/cm^2 illuminations, which is higher than that of bare TiO_2 nanotube photoanode (0.3 %).

Keywords: TiO_2 nanotube, ZnS nanoparticles, Flexible dye sensitized solar cells, Anodization, Sensitizer, Light harvesting.

INTRODUCTION

Due to their simple structure, flexibility, low production cost and wide range of application dye-sensitized solar cells (DSSCs) have been broadly studied as an alternate to silicon-based solar cells, since their discovery in 1991. However, the low efficiency of DSSCs compared to that of silicon-based cells has limited their commercial implementation. In order to realize next generation solar cells there is a critical need to increase the efficiency of DSSCs [1,2]. The composition of DSSCs are (a) electrode film layer (TiO_2), covered by a mono-layer of dye molecules, which absorbs the incident solar energy; (b) the conductive transparent oxide layer that accelerates charge transfer from the electrode layer; (c) counter electrode layer made of such as Pt , C, PANI, *etc*. and (d) the redox electrolyte layer for reducing the level of energy supplied from the dye molecules. Many research efforts to improve the efficiency of DSSCs have mainly been focused on enhancements of the each DSSC component [1].

Anatase TiO_2 is essential inorganic material that is considered the prominent cathode electrode material in solar cells and is capable of efficiently harvesting light. Among different shapes of titania, TiO_2 nanotubes (TNT) have gained a lot of interest in the last decades [3]. In DSSC, the photo-excited electrons of the dye molecules are transferred to TiO_2 conduction band, which is taken out through an external circuit using an anode electrode and a counter electrode in the presence of a liquid or solid redox electrolyte [4].

The optimization of counter-electrodes has been achieved to encourage the conversion efficiency of liquid electrolyte DSSCs. For this purpose, new routes of sensitization and surface passivation were used, such as depositing a thin layer [insulating metal oxides (Al_2O_3), ZnS or SiO_2] on the surface of ZnO or TiO_2. The deposition of zinc sulphide (ZnS) layer on the surface of TiO_2 photoanode taking advantage of the easy preparation and the remarkable enhancement of the efficiency achieved. Also, the deposition of ZnS layer between TiO_2 and dye molecules is suitable to enhance the electron injection and decrease the charge recombination [5].

The DSSCs fabrication can be changed from traditional glass substrates to either flexible plastic or metal and can be fabricated in different combination. The flexible DSSCs can be prepared in many basic configurations. There are significant challenges associated with each type of configuration. For example, if the materials could be deposited or coated using low temperature paste or inks the whole cell assembly can be fabricated on transparent conducting oxide coated flexible plastic sheets like traditional glass based DSSC. However, this config-

uration needed careful optimization to achieve maximum output power since the cell is illuminated from the counter electrode side and the light is absorbed by semi-transparent catalyst and electrolyte [6]. Flexible DSSC fabricated on conductive plastics substrate or metal foil renders solar cell with conformabilities to uneven surfaces. It can be particularly designed for specific forms to satisfy the special shape requirements, such as attachment to the surface of windows, clothing and portable electronic devices [7].

In this study, a composite material, TiO_2 nanotube arrays/ZnS nanoparticles (TNT/ZnS NPs) was assembled by the deposition of ZnS nanoparticles onto the anodized TNT arrays *via* sequential chemical bath deposition method. Flexible DSSC with dimension of (2 × 2.5) cm were fabricated, characterized and optimized.

EXPERIMENTAL

To prepare TiO_2 nanotube photo-anode using anodization method, titanium foil substrate was first cleaned with deionized water, ethanol and acetone for 10 min by using an ultrasonic bath. Anodization process of titanium foil was achieved in a two-electrode cell with titanium foil acting as the working electrode, while a Pt as the counter electrode and 0.5 wt % NH_4F dissolved in 50 mL anhydrous ethylene glycol, with 4 vol % water solution as the electrolyte at 30 V. After that the samples are rinsed in ethanol and dried. Then, after many experiments to obtain the optimum annealing temperature, the samples annealed at 550 ºC for 2 h.

The deposition of ZnS nanoparticles onto the annealed TiO_2 nanotube layer was done by sequential chemical bath deposition method. The ZnS nanoparticles were prepared by two chemical solutions of 0.1M: the first one is prepared by dissolving 1.36g of zinc chloride powder in 100 mL distilled water. Ammonia was added to the mixture to adjust the pH of the solution to the required levels of (pH=7.5, 8.5, and 9.5). The second solution is prepared by dissolving 0.78g from sodium sulfide powder Na_2S in 100 mL deionized water. The TNT sample is immersed in the cationic precursor for 3 min where adsorption of Zn^{2+} ions takes place on the surface of TNT and unadsorbed ions were removed by rinsing the TNT in deionized water for 10 s. Then, this sample is immersed in an anionic precursor for 3 min. The sulphide ions (S^{2-}) ions are reacted with Zn^{2+} ions. The loosely bound ions were removed by rinsing the sample in deionized water for 10 s. Thus, one layer of ZnS is formed, this completes one sequential-chemical bath deposition (CBD) cycle. These sequent sequential-chemical bath deposition cycles were repeated 5 times until the required film thickness was reached [8].

The structural properties are studied using X-ray diffraction. The morphology and surface features of photo-anodes were determined by using atomic force microscopy and field emission scanning electron microscope (FE-SEM) operated at 15 kV. The elemental composition of TNT/ZnS nanoparticles photo-anodes was identified by energy-dispersive X-ray spectroscopy (EDX). The photo-current density-voltage (J-V) characteristics of the assembled flexible DSSCs were found using a solar simulator (80 mW cm^{-2}) illumination. These measurements are done using the configuration presented in Fig. 1.

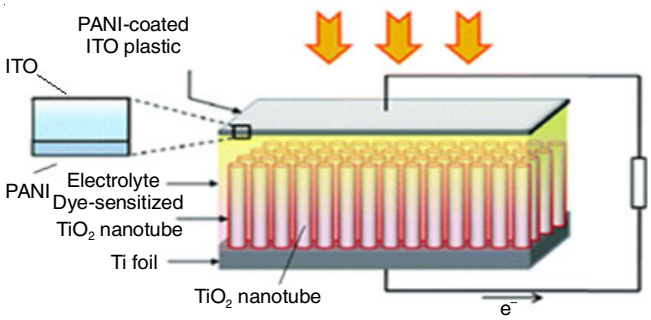

Fig. 1. A Schematic diagram of the assembled flexible DSSC

RESULTS AND DISCUSSION

Structural studies for electropolymerized polyaniline (PANI) on indium tin oxide (ITO) plastic counter electrode

X-Ray diffraction: The crystal structure of deposited PANI on indium tin oxide plastic substrate was examined by X-ray diffraction patterns (XRD) as shown in Fig. 2. In the XRD pattern of PANI, the characteristic peaks appearing at 2θ of 9.49º, 19.28º, 25.7º and 29.2º which correspond to (001), (020) and (200) and (022) crystal planes of PANI. This result is comparable with results of reported literature [9].

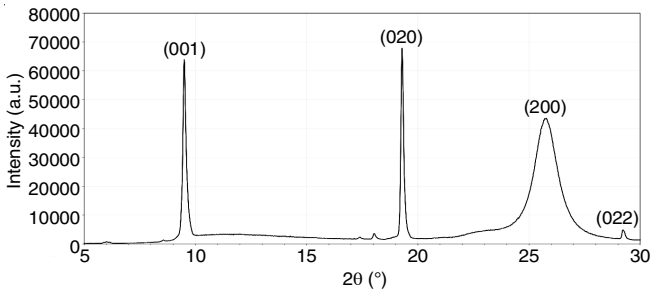

Fig. 2. XRD spectra of electropolymerized PANI

FT-IR: The Fourier transformation infrared spectrum of electropolymerized PANI is shown in Fig. 3. In this spectrum, the band observed at 3429.2 cm^{-1} is due to O-H stretching vibrations. The polymer shows the absorption band at 2879.52 cm^{-1} is due to symmetric C-H stretching vibrations [9]. The peaks at 1564.16 and 1488.94 cm^{-1} are attributed to C=C stretching of quinonoid rings and C=C stretching of benzenoid rings, respectively [10]. The characteristic peak at 1236.29 and 1299.93 cm^{-1} are due to C-N stretching of primary aromatic amines [9,11].

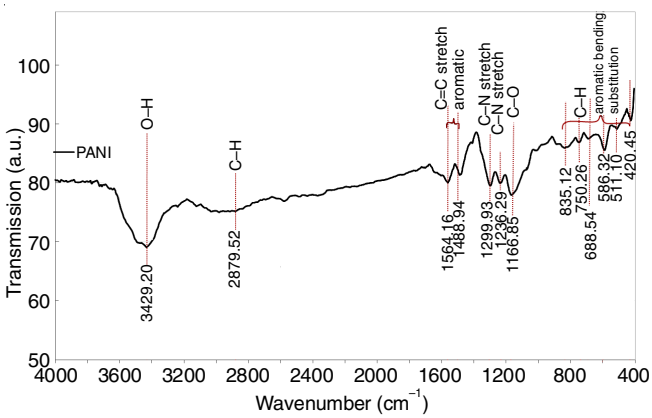

Fig. 3. Infrared spectrum of electropolymerized PANI

Absorption spectrum for Ru-N719 dye: In DSSCs, the sensitizer plays an essential role and is responsible for the electric current generation by harvesting the solar irradiation and injecting the excited electrons into the TNT conduction band [5]. The optical properties of the dye were measured by UV-visible spectroscopy. The absorption spectrum of Ru-N719 dye is shown in Fig. 4. Two main peaks were observed at 384 and 527 nm. This result is comparable with the results obtained by Arifin *et al.* [12].

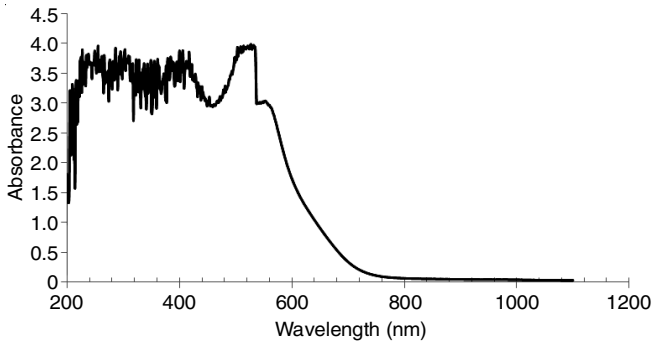

Fig. 4. Absorbance spectra of Ru-N719 dye as function of wavelength

Structural properties of TiO_2 nanotubes (TNT) prepared by anodizing process

X-Ray diffraction: X-Ray diffraction patterns of bare TNT and TNT/ ZnS nanoparticles photoanode for anodization time of 1 h on titanium foil substrate (before and after annealing of TNT) are shown in Figs. 5 and 6. The XRD measurements were

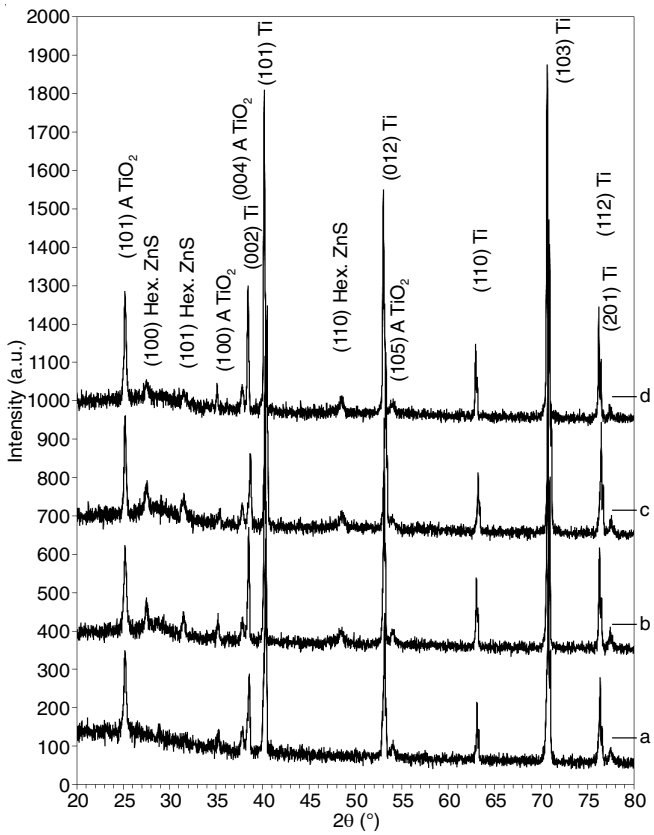

Fig. 5. XRD patterns for flexible DSSC photoanodes for anodization time (1 h) and (before annealing): (a) bare TiO_2 nanotubes, (b) TNT/ ZnS NPs (pH = 7.5), (c) TNT/ ZnS NPs (pH = 8.5) and (d) TNT/ ZnS NPs (pH = 9.5)

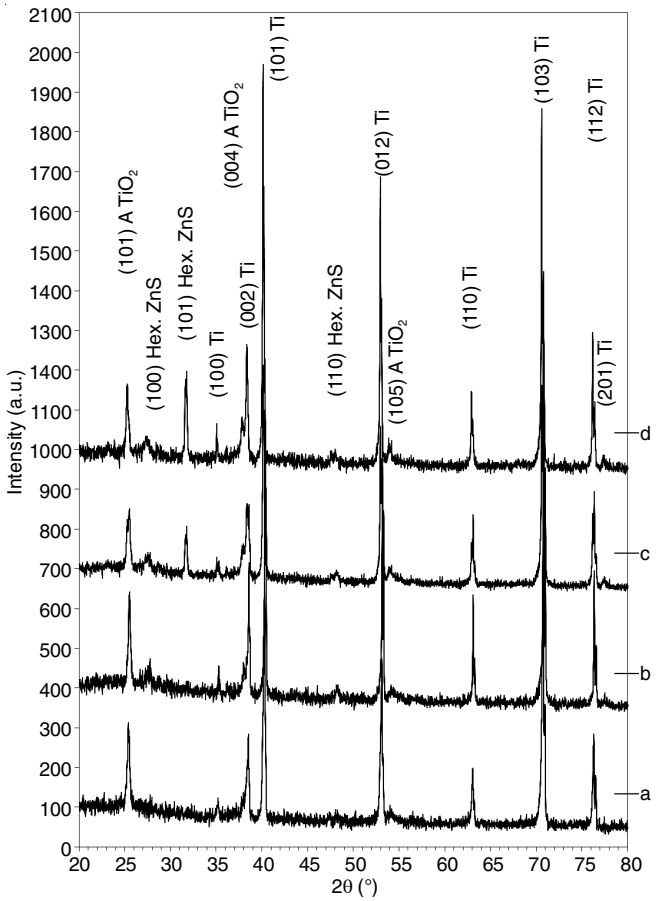

Fig. 6. XRD patterns for flexible DSSC photoanodes for anodization time (1 h) and (after annealing): (a) bare TiO_2 nanotubes, (b) TNT/ZnS NPs (pH = 7.5), (c) TNT/ZnS NPs (pH = 8.5) and (d) TNT/ZnS NPs (pH = 9.5)

studied to investigate the effect of TNT annealing at 550 ºC for 2 h and the variation of pH values of ZnS nanoparticles on the crystallinity of photoanode.

As shown in Fig. 5, X-ray diffraction patterns of TNT before annealing of TNT films, identified an anatase structure without any new phases. Also, three diffraction peaks were observed at around 2θ = 25.172º, 37.784º and 54.03º, which are indicated to (101), (004) and (105) crystal planes (JCPDS card no:96-900-9087), respectively. The diffraction peaks of ZnS nanoparticles were observed at around 2θ = 27.4º, 31.5º and 48.4º (JCPDS card no: 96-901-3421), indicating hexagonal structure for the synthesized nanocrystals. The decreasing peak intensity of TiO_2 nanotube of pH value 7.5 and 8.5 of ZnS nanoparticles is resulted from the insertion of ZnS on TiO_2 nanotube, or some amorphous substance formation on the film surface of TiO_2 nanotubes [5] and this is caused by the quantum confinement effect which leads to the decease of size of ZnS nanoparticles. Whereas, the intensity of TiO_2 nanotube peak for pH value equal to 9.5 of ZnS nanoparticles is increasing, which is caused by increasing of the particle size of ZnS nanoparticles and leads to the accumulation of nanoparticles at the surface of TiO_2 nanotube film.

The sizes of nanocrystalline were calculated using Debye-Scherrer formula. The average crystalline size was found to be 25.7 nm for bare TiO_2 nanotube and ZnS coated TiO_2 nanotube from the prominent (101) diffracted peak. Table-1 showed

TABLE-1
X-RAY DIFFRACTION PATTERN PARAMETERS FOR FLEXIBLE DSSC PHOTOANODES, ANODIZATION TIME (1 h) AND (BEFORE ANNEALING)

pH	2θ (°)	FWHM (°)	d_{hkl} exp. (Å)	G.S. (nm)	hkl	d_{hkl} std. (Å)	Phase	Card No.
TNT (bare)	25.172	0.3694	3.5351	22.0	(101)	3.5169	Anatase	96-900-9087
	35.251	0.4221	2.5440	19.7	(100)	2.5525	Ti	96-900-8518
	37.784	0.4749	2.3791	17.7	(004)	2.3785	Anatase	96-900-9087
	38.470	0.3694	2.3382	22.8	(002)	2.3411	Ti	96-900-8518
	40.158	0.3166	2.2437	26.7	(101)	2.2415	Ti	96-900-8518
	53.140	0.3167	1.7222	28.0	(012)	1.7255	Ti	96-900-8518
	54.037	0.4222	1.6957	21.1	(105)	1.7001	Anatase	96-900-9087
	63.114	0.3694	1.4719	25.2	(110)	1.4738	Ti	96-900-8518
	70.818	0.4222	1.3295	23.1	(103)	1.3316	Ti	96-900-8518
	76.359	0.4221	1.2462	23.9	(112)	1.2473	Ti	96-900-8518
	77.520	0.6333	1.2304	16.1	(201)	1.2313	Ti	96-900-8518
7.5	25.172	0.3166	3.5351	25.7	(101)	3.5169	Anatase	96-900-9087
	27.441	0.3166	3.2477	25.8	(100)	3.2710	Hex ZnS	96-901-3421
	31.504	0.3694	2.8375	22.3	(101)	2.8918	Hex ZnS	96-901-3421
	35.198	0.2638	2.5477	31.6	(100)	2.5525	Ti	96-900-8518
	37.836	0.3694	2.3759	22.7	(004)	2.3785	Anatase	96-900-9087
	38.470	0.2639	2.3382	31.9	(002)	2.3411	Ti	96-900-8518
	40.158	0.2639	2.2437	32.1	(101)	2.2415	Ti	96-900-8518
	48.391	0.6860	1.8795	12.7	(110)	1.8885	Hex ZnS	96-901-3421
	52.929	0.2638	1.7285	33.6	(012)	1.7255	Ti	96-900-8518
	53.984	0.4222	1.6972	21.1	(105)	1.7001	Anatase	96-900-9087
	63.008	0.3694	1.4741	25.2	(110)	1.4738	Ti	96-900-8518
	70.765	0.4222	1.3303	23.1	(103)	1.3316	Ti	96-900-8518
	76.306	0.3166	1.2469	31.9	(112)	1.2473	Ti	96-900-8518
	77.414	0.5277	1.2318	19.3	(201)	1.2313	Ti	96-900-8518
8.5	25.172	0.3166	3.5351	25.7	(101)	3.5169	Anatase	96-900-9087
	27.493	0.5277	3.2416	15.5	(100)	3.2710	Hex ZnS	96-901-3421
	31.398	0.5805	2.8468	14.2	(101)	2.8918	Hex ZnS	96-901-3421
	35.356	0.4222	2.5366	19.7	(100)	2.5525	Ti	96-900-8518
	37.731	0.3694	2.3823	22.7	(004)	2.3785	Anatase	96-900-9087
	38.628	0.3167	2.3290	26.6	(002)	2.3411	Ti	96-900-8518
	40.264	0.3694	2.2381	22.9	(101)	2.2415	Ti	96-900-8518
	48.496	0.6332	1.8756	13.8	(110)	1.8885	Hex ZnS	96-900-8518
	53.193	0.3694	1.7206	24.1	(012)	1.7255	Ti	96-900-8518
	54.037	0.6333	1.6957	14.1	(105)	1.7001	Anatase	96-900-9087
	63.114	0.3694	1.4719	25.2	(110)	1.4738	Ti	96-900-8518
	70.765	0.4750	1.3303	20.5	(103)	1.3316	Ti	96-900-8518
	76.359	0.3694	1.2462	27.4	(112)	1.2473	Ti	96-900-8518
	77.467	0.5277	1.2311	19.3	(201)	1.2313	Ti	96-900-8518
9.5	25.172	0.3166	3.5351	25.7	(101)	3.5169	Anatase	96-900-9087
	27.493	0.5804	3.2416	14.1	(100)	3.2710	Hex ZnS	96-901-3421
	31.451	0.4750	2.8421	17.4	(101)	2.8918	Hex ZnS	96-901-3421
	35.092	0.2111	2.5551	39.5	(100)	2.5525	Ti	96-900-8518
	37.784	0.3167	2.3791	26.5	(004)	2.3785	Anatase	96-900-9087
	38.417	0.2111	2.3413	39.9	(002)	2.3411	Ti	96-900-8518
	40.106	0.2111	2.2465	40.1	(101)	2.2415	Ti	96-900-8518
	48.443	0.4750	1.8776	18.3	(110)	1.8885	Hex ZnS	96-901-3421
	52.982	0.2638	1.7269	33.6	(012)	1.7255	Ti	96-900-8518
	54.037	0.6861	1.6957	13.0	(105)	1.7001	Anatase	96-900-9087
	62.902	0.3166	1.4763	29.4	(110)	1.4738	Ti	96-900-8518
	70.660	0.2638	1.3320	36.9	(103)	1.3316	Ti	96-900-8518
	76.201	0.2638	1.2484	38.3	(112)	1.2473	Ti	96-900-8518
	77.309	0.3694	1.2332	27.5	(201)	1.2313	Ti	96-900-8518

the X-ray diffraction parameters for flexible DSSC photoanodes (before annealing).

Fig. 6 shows the XRD patterns after annealing of TNT films. It was found that TiO_2 nanotubes films have an anatase structure (JCPDS: 96-900-9087). Also, three diffraction peaks were observed at around 25.38º, 37.9º and 54º, which are correspond to (101), (004) and (105) crystal planes respectively. Meanwhile, TNT/ZnS nanoparticles films with different pH values for ZnS nanoparticles exhibit weak diffraction peaks at 2θ = 27.7º, 31.7º and 48.1º correspond to (100), (101) and (110) hexagonal form of ZnS nanoparticles (JCPDS: 96-901-3421).

Upon annealing at high temperature of 550 ºC of TNT films, the changes in diffraction peaks and the full width at half maximum (FWHM) were used to calculate the crystallite size by using the Debye-Scherrer's equation. The diffraction peaks of TNT at 2θ = 25.52º and ZnS at 2θ = 27.7º were used as the reference peaks. The crystallite size value of TNT was 24.4 nm, while the crystallite size of TNT/ZnS nanoparticles

with different values of pH for ZnS nanoparticles was 21.6 nm, and upon annealing at 550 ºC, the crystallite size had decreased from 25.7 to 21.6 nm. Table-2 shows the X-ray diffraction pattern parameters for flexible DSSC photoanodes (after annealing).

Surface morphology of electrodes using atomic force microscopy technique: Atomic force microscopy technique (AFM) is a method to analyze films surface topography. Fig. 7a-b shows two dimensional and three dimensional AFM images for the samples were anodized for 1 h at 30 V, using an electrolyte consisting of 0.5 wt. % NH_4F, 4 vol % deionized water and 50 vol % of ethylene glycol. These figures illustrate the AFM images of bare TNT and TNT/ZnS nanoparticles electrodes on titanium foil substrate and for pH of ZnS nanoparticles equal to (7.5, 8.5 and 9.5). From these results, honeycombs structures were recorded.

Other topography parameters are the root mean square roughness (Sq), average particle size, and ten point height (Sz) which valued from the granularity accumulation distribution, as shown in Table-3.

Scanning electron microscopy (SEM): The SEM images report samples that were anodized for 1 h at 30 V, using an electrolyte consisting of 0.5 wt. % NH_4F, 4 vol % deionized water and 50 vol % of ethylene glycol. Fig. 8 illustrated the SEM images of bare TNT and TNT/ZnS nanoparticles films

TABLE-2
X-RAY DIFFRACTION PATTERN PARAMETERS FOR FLEXIBLE DSSC PHOTOANODES, ANODIZATION TIME (1 h) AND (AFTER ANNEALING)

pH	2θ (°)	FWHM (°)	d_{hkl} exp. (Å)	G.S. (nm)	hkl	d_{hkl} std. (Å)	Phase	Card No.
TNT (bare)	25.385	0.3336	3.5058	24.4	(101)	3.5169	Anatase	96-900-9087
	35.203	0.3336	2.5474	25.0	(100)	2.5525	Ti	96-900-8518
	38.539	0.3336	2.3342	25.2	(002)	2.3411	Ti	96-900-8518
	40.302	0.3336	2.2360	25.4	(101)	2.2415	Ti	96-900-8518
	53.122	0.2383	1.7227	37.3	(012)	1.7255	Ti	96-900-8518
	54.170	0.5719	1.6918	15.6	(105)	1.7001	Anatase	96-900-9087
	63.034	0.2859	1.4735	32.6	(110)	1.4738	Ti	96-900-8518
	70.850	0.3813	1.3289	25.6	(103)	1.3316	Ti	96-900-8518
	76.283	0.3336	1.2472	30.3	(112)	1.2473	Ti	96-900-8518
7.5	25.528	0.3336	3.4865	24.4	(101)	3.5169	Anatase	96-900-9087
	27.720	0.5242	3.2156	15.6	(100)	3.2710	Hex ZnS	96-901-3421
	31.771	0.5242	2.8142	15.8	(101)	2.8918	Hex ZnS	96-901-3421
	35.250	0.2859	2.5440	29.2	(100)	2.5525	Ti	96-900-8518
	38.586	0.2383	2.3314	35.3	(002)	2.3411	Ti	96-900-8518
	40.350	0.2383	2.2335	35.5	(101)	2.2415	Ti	96-900-8518
	48.118	0.5719	1.8895	15.2	(110)	1.8885	Hex ZnS	96-901-3421
	53.169	0.2383	1.7213	37.3	(012)	1.7255	Ti	96-900-8518
	54.170	0.6672	1.6918	13.4	(105)	1.7001	Anatase	96-900-9087
	63.082	0.1906	1.4725	48.9	(110)	1.4738	Ti	96-900-8518
	70.850	0.3336	1.3289	29.2	(103)	1.3316	Ti	96-900-8518
	76.330	0.3336	1.2466	30.3	(112)	1.2473	Ti	96-900-8518
	77.474	0.3812	1.2310	26.7	(201)	1.2313	Ti	96-900-8518
8.5	25.481	0.4289	3.4929	19.0	(101)	3.5169	Anatase	96-900-9087
	27.577	0.5719	3.2319	14.3	(100)	3.2710	Hex ZnS	96-901-3421
	31.676	0.3813	2.8225	21.7	(101)	2.8918	Hex ZnS	96-901-3421
	35.060	0.3336	2.5574	25.0	(100)	2.5525	Ti	96-900-8518
	37.967	0.4766	2.3680	17.6	(004)	2.3785	Anatase	96-900-9087
	38.348	0.3336	2.3453	25.2	(002)	2.3411	Ti	96-900-8518
	40.111	0.1907	2.2462	44.3	(101)	2.2415	Ti	96-900-8518
	48.213	0.4765	1.8860	18.3	(110)	1.8885	Hex ZnS	96-901-3421
	52.979	0.2860	1.7270	31.0	(012)	1.7255	Ti	96-900-8518
	54.075	0.4289	1.6946	20.8	(105)	1.7001	Anatase	96-900-9087
	62.987	0.2860	1.4745	32.6	(110)	1.4738	Ti	96-900-8518
	70.612	0.2859	1.3328	34.0	(103)	1.3316	Ti	96-900-8518
	76.378	0.2860	1.2459	35.3	(112)	1.2473	Ti	96-900-8518
	77.427	0.4766	1.2316	21.4	(201)	1.2313	Ti	96-900-8518
9.5	25.290	0.3812	3.5188	21.4	(101)	3.5169	Anatase	96-900-9087
	27.292	0.6672	3.2651	12.3	(100)	3.2710	Hex ZnS	96-901-3421
	31.628	0.3336	2.8266	24.8	(101)	2.8918	Hex ZnS	96-901-3421
	35.060	0.1906	2.5574	43.7	(100)	2.5525	Ti	96-900-8518
	37.824	0.3336	2.3766	25.2	(004)	2.3785	Anatase	96-900-9087
	38.348	0.2383	2.3453	35.3	(002)	2.3411	Ti	96-900-8518
	40.111	0.1907	2.2462	44.3	(101)	2.2415	Ti	96-900-8518
	48.022	0.6195	1.8930	14.0	(110)	1.8885	Hex ZnS	96-901-3421
	52.979	0.2383	1.7270	37.2	(012)	1.7255	Ti	96-900-8518
	53.884	0.3812	1.7001	23.4	(105)	1.7001	Anatase	96-900-9087
	62.891	0.2383	1.4766	39.1	(110)	1.4738	Ti	96-900-8518
	70.612	0.2859	1.3328	34.0	(103)	1.3316	Ti	96-900-8518
	76.188	0.2860	1.2486	35.3	(112)	1.2473	Ti	96-900-8518
	77.284	0.3812	1.2336	26.7	(201)	1.2313	Ti	96-900-8518

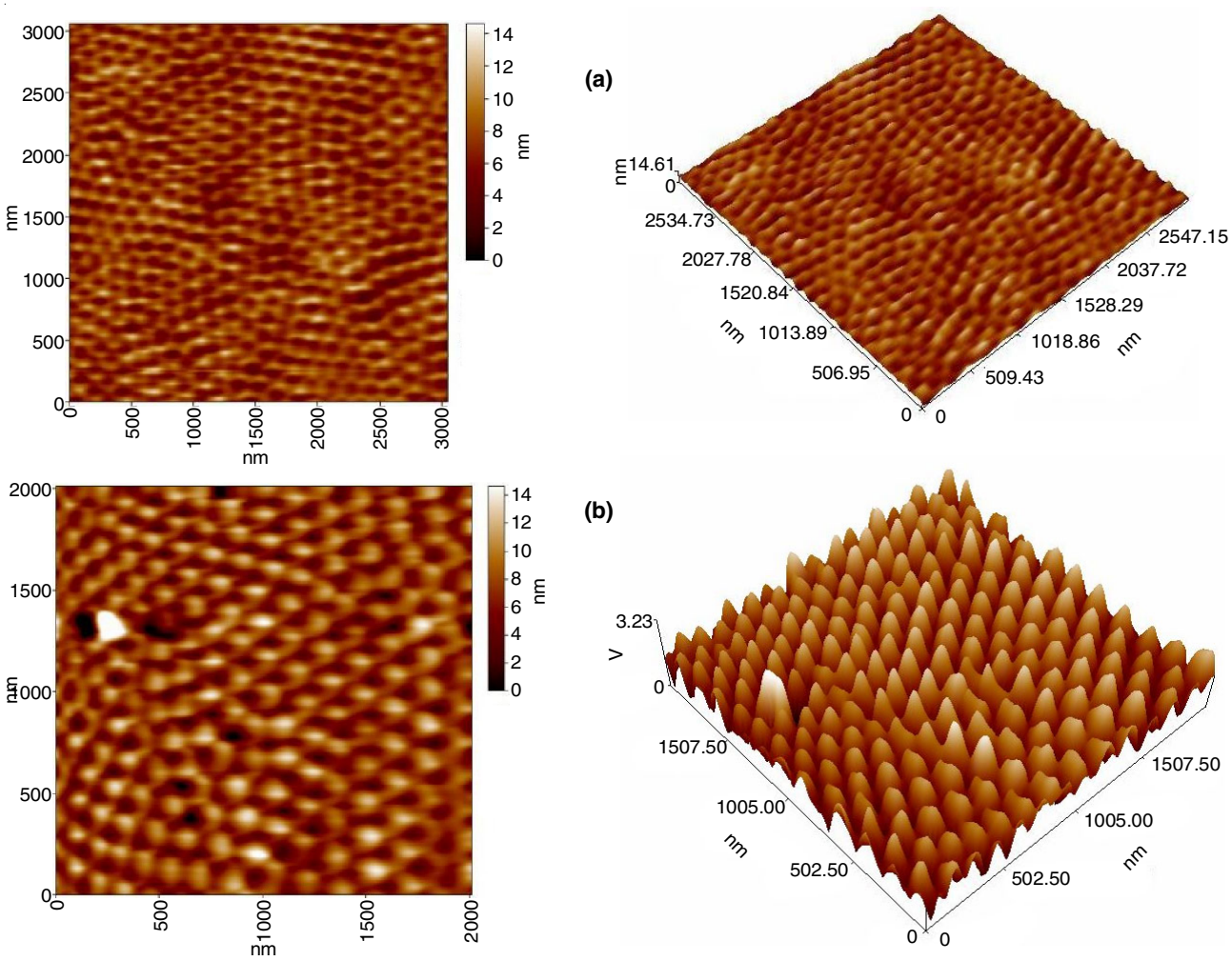

Fig. 7. 2D & 3D AFM images of (a) bare TNT and (b) TNT/ZnS NPs electrodes and for pH = 8.5

TABLE-3
SURFACE TOPOGRAPHY PARAMETERS OBTAINED FROM AFM
ANALYSIS FOR BARE TNT AND TNT/ZnS NPs ELECTRODES SURFACES

Sample	pH	Sa (nm)	Sq (nm)	Sz (nm)	Ave. G.S. (nm)
TNT (bare)	–	0.36	0.45	2.95	91.12
TNT/ZnS NPs	8.5	1.82	2.3	14.2	94.55

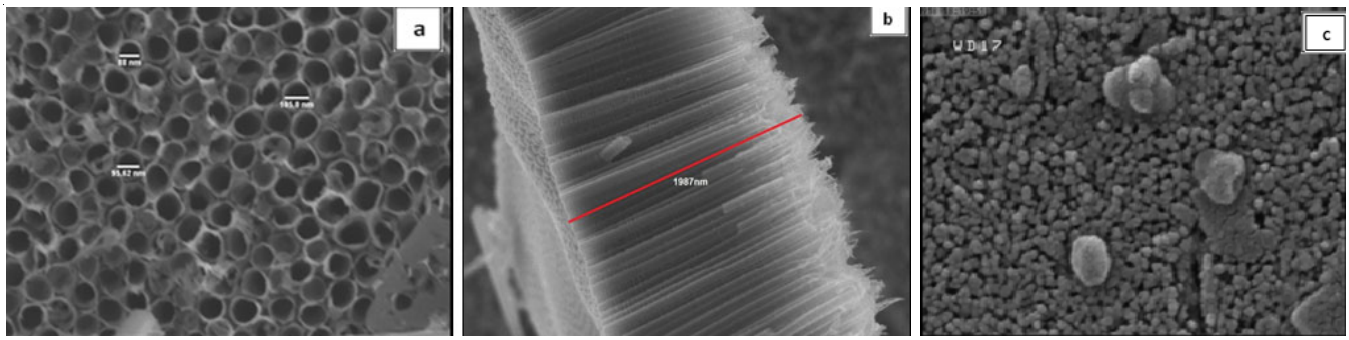

Fig. 8. SEM images of the bare TiO_2 nanotubes film prepared by anodizing in (NH_4F of 0.5 wt. %, 4 vol % deionized water and 50 vol % of ethylene glycol), with anodizing potential of 30 V for 1 h, (a) top view, (b) cross-sectional view and (c) TNT/ZnS NPs photoanode

on titanium foil substrate, and for pH value of ZnS nanoparticles equal to 8.5. Before the deposition of ZnS nanoparticles layer, the TNT film was annealed at 550 ºC for 2 h. The SEM images were taken to understand the deposition effect of ZnS nanoparticles layers on the morphological growth of TiO_2 nanotubes. Fig. 8a-b shows the self-organized TNT produced on titanium foil *via* electrochemical anodization at 30 V. The measurements of the tube parameters (length, diameter and wall thickness)

were conducted on SEM images revealed the length nearly (2 μ), the tube diameter around 96 nm while the wall thickness about 20 nm. In comparison with bare TNT film (Fig. 8c), non- uniform distribution of deposited ZnS nanoparticles was formed on the surface of TiO_2 nanotubes and there are gaps between the nanoparticles. As seen in this figure, large size of ZnS nanoparticles at the surface of TNT is observed. However, the annealing temperature at 550 ºC of TNT has blocked the mouth of nanotubes before the deposition of ZnS nanoparticles.

Composition analysis: To identify the elemental compositions of the prepared electrodes on titanium foil substrates energy-dispersive X-ray spectroscopy (EDX) analysis was used. Fig. 9 shows the representative EDX pattern of Ti, O, Zn and S elements which confirms the formation TNT/ZnS photoanode. This means that the film quality is good since no other compounds is observed in the film (Table-4).

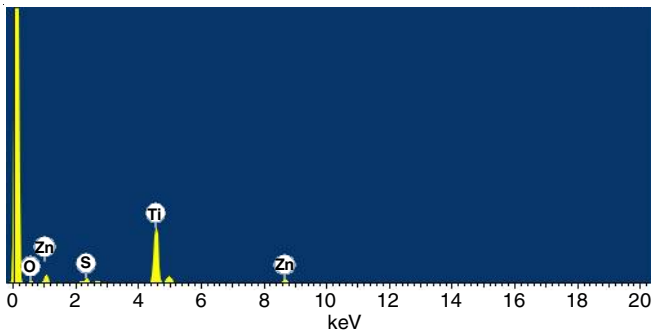

Fig. 9. EDX spectrum of TNT/ZnS NPs photoanode

TABLE-4
COMPOSITION OF TNT/ZnS NPs
PHOTOANODE DETERMINED BY EDX

Element	Weight (%)	Atomic (%)
O K	26.57	52.96
S K	2.17	2.15
Ti K	56.90	37.88
Zn K	14.36	7.01
Totals	100.00	

J-V Characterization of assembled flexible DSSCs for anodization time 1 h (before and after annealing): All types of the assembled flexible DSSCs from mixed combination of PANI/ITO plastic catalyzed cathode and different active anodes were subjected to J-V characterization by fast scan with two electrodes potentiostat, to evaluate all parameters of each of them; current short circuit (J_{sc}), voltage of open circuit (V_{oc}), maximum cell power (P_{max}), the fill factor (FF) and power conversion efficiency (η) were calculated using two electrodes potentiostatic measurements. Fig. 10 illustrates the J-V curves under an illumination of 80 mW/cm^2 conditions for all the assembled

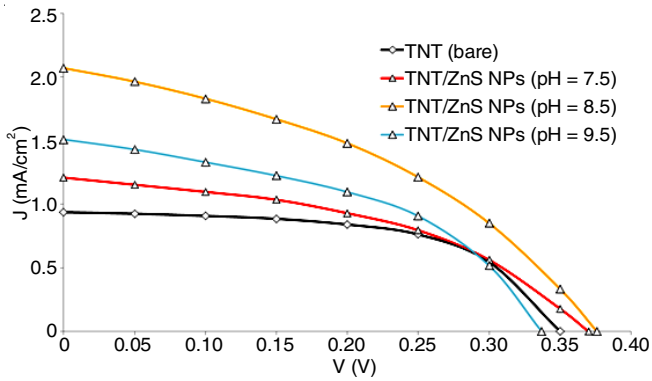

Fig. 10. J-V characteristics of the assembled flexible DSSCs from PANI/ ITO plastic sheet as catalyzed cathodes and different photoanodes (before annealing)

flexible DSSCs of bare TNT photoanode and TNT/ZnS nanoparticles with different pH values of ZnS nanoparticles films, and without thermal annealing treatment of TNT films. This figure reflects the effect of photoanode materials on the performance of the assembled flexible DSSCs. Data for all the experiments are summarized in Table-5.

It is apparent from the figure that using bare TiO_2 nanotube (TNT) as a photoelectrode and PANI/ITO as a counter electrode, the fabricated cell exhibited J_{sc}, V_{oc} and FF values of (0.94 mA cm^{-2}, 0.35 V and 0.59) respectively, resulting in a low efficiency of 0.24 %. The electrocatalytic activity of TNT electrode was very low, which provides low current density. Under continuous illumination, TNT/ZnS nanoparticles of ZnS of pH value equal to 8.5 electrode exhibited the highest conversion efficiency of 0.4 % in KI/I_2 electrolyte, which is higher than that of other photoelectrodes. The fabricated cell exhibited J_{sc}, V_{oc} and FF values of (2.1 mA cm^{-2}, 0.38 V and 0.41), respectively. It can be concluded that the positive influence of ZnS nanoparticles deposition on TNT layer resulted in the enhancement of power conversion efficiency, which results in improved photo-electron harvesting efficiency of photoanode and relatively low resistivity. However, combination of TNT/ZnS nanoparticles shows considerably better photocatalytic activity than bare TNT film.

The high photocurrent density (J_{sc} = 2.1 mA cm^{-2}) leads to higher power conversion efficiency for TNT/ZnS nanoparticles of ZnS pH value equal to 8.5 electrode than bare TNT photoanode. This result proposes that the replacement of Ti^{2+} by Zn^{2+} ions on the surface reinforced and increased in the surface stability compared to the bare TNT photoanode. Consequently the dye molecules are effectively adsorbed on the electrode surface, which is caused by the reduction of ZnS-dye aggregations. In contrast, the performance of TNT/ZnS nanoparticles of ZnS pH values equal to 7.5 and 9.5 photoelectodes (η = 0.25 %, J_{sc} = 1.2 mA cm^{-2}, V_{oc} = 0.37 V and FF = 0.45) and (η = 0.29 %,

TABLE-5
PARAMETERS OF THE ASSEMBLED FLEXIBLE DSSCs FROM PANI/ ITO PLASTIC SHEET AS CATALYZED CATHODES AND DIFFERENT PHOTOANODES (BEFORE ANNEALING)

Cathode	Photoanode	pH value of ZnS NPs	J_{sc} (mA/cm^2)	V_{oc} (V)	J_m (mA)	V_m (v)	F.F.	η (%)
PANI/ITO plastic	TNT (bare)	–	0.940	0.350	0.720	0.270	0.591	0.243
PANI/ITO plastic	TNT/ZnS NPs	7.5	1.200	0.370	0.800	0.250	0.450	0.250
PANI/ITO plastic	TNT/ZnS NPs	8.5	2.100	0.375	1.300	0.250	0.413	0.406
PANI/ITO plastic	TNT/ZnS NPs	9.5	1.460	0.330	0.880	0.260	0.475	0.286

J_{sc} = 1.4 mA cm^{-2}, V_{oc} = 0.33 V and FF = 0.48), respectively, were lower than that with TNT/ZnS nanoparticles of ZnS pH value equal to 8.5. The decrease in J_{sc} for TNT/ZnS nanoparticles of ZnS pH values equal to 7.5 and 9.5 photoelectodes, is due to its lower conductivity and catalytic activity for I_3^- reduction. However, the effect of pH values of ZnS nanoparticles, which deposited on TNT layer will change the optical band gap and the insulating properties of TNT films, which significantly reduces the rate of electron transfer from the photoanode to titanium foil and then to external circuit.

The possible electron transfer mechanism in the photoanode is schematically represented in Fig. 11. In Fig. 11a, during the electron injection there are undesirable side processes. When the electrons injected to the conduction band (CB) of TNT, it may reduce either the oxidized dye (recombination), or I_3^- in the solution (dark current). These two processes reduce the short-circuit photocurrent density (J_{sc}). Due to a higher band gap of ZnS nanoparticles (3.75 eV) for pH= 8.5 is attributed to the quantum confinement effect, the excited electrons are confined inside the TNT and the holes are localized in ZnS nanoparticles layer. Also, the deposition of ZnS nanoparticles layer between TNT and dye molecules can successfully avoid the formation of insulating [dye-Zn^{2+}] complexes, which is important for improving the device's stability and the decrease of charge recombination. Also, it can be noticed from Fig. 11b that the deposition of ZnS nanoparticles layer on top of TNT leads to a more efficient photocatalyst than pure TNT.

In addition, ZnS nanoparticles film makes a blocking layer to protect TNT from the outer dye/electrolyte, and provides physical separation of the injected electrons in TNT from the positively charged dye/electrolyte, thus reducing the interfacial recombining to achieve a high photovoltaic performance. It is illustrated from the J-V plots in Fig. 10 and Table-5 that an efficiency of around 0.4 % is obtained by an optimized combination of these materials. The efficiency of the cell is improved from 0.24 to 0.4 % by introducing ZnS nanoparticles layer between TNT and dye. Therefore, the electron lifetime is improved with the introduction of ZnS nanoparticles layer. This result is comparable with other results obtained earlier [5].

Fig. 12 presents the J-V characteristics under an illumination of 80 mW/cm^2 conditions of all the assembled flexible DSSCs of bare TNT photoanode and TNT/ZnS nanoparticles with different pH values photoanodes with TNT annealed at 550 ºC for 2 h before the deposition of ZnS nanoparticles layer. This figure shows the effect of photoanode materials and the annealing of TNT on the performance of the assembled flexible DSSCs. The corresponding values of J_{sc}, V_{oc}, FF and PCE for these devices are summarized in Table-6.

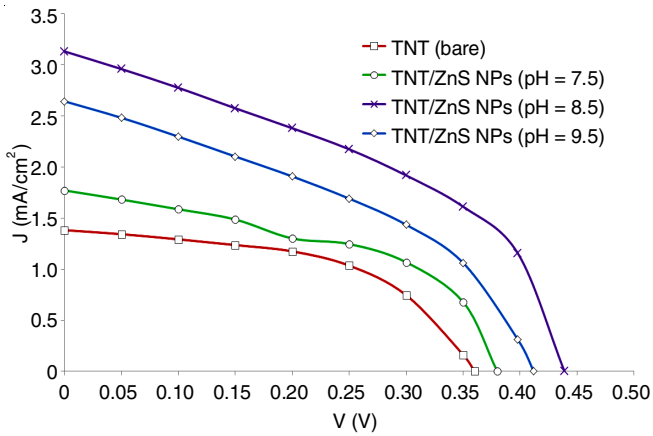

Fig. 12. J-V characteristics of the assembled flexible DSSCs from PANI/ ITO plastic sheet as catalyzed cathodes and different photoanodes, anodization time 1 h and (after annealing)

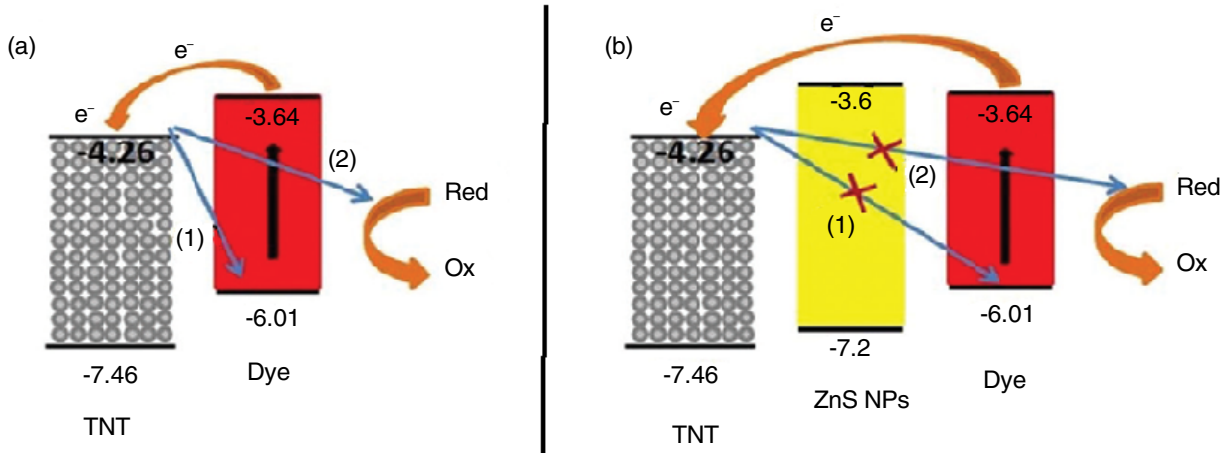

Fig. 11. Schematic diagram of flexible DSSC (a) without and (b)with ZnS NPs blocking layer

TABLE-6
PARAMETERS OF THE ASSEMBLED FLEXIBLE DSSCs FROM PANI/ ITO PLASTIC SHEET AS CATALYZED CATHODES AND DIFFERENT PHOTOANODES, ANODIZATION TIME (1 h) AND (AFTER ANNEALING)

Cathode	Photoanode	pH value of ZnS NPs	J_{sc} (mA/cm^2)	V_{oc} (V)	J_m (mA)	V_m (v)	F.F.	η (%)
PANI/ITO plastic	TNT (bare)	–	1.400	0.360	1.000	0.260	0.516	0.300
PANI/ITO plastic	TNT/ZnS NPs	7.5	1.800	0.380	1.240	0.265	0.480	0.330
PANI/ITO plastic	TNT/ZnS NPs	8.5	3.100	0.440	2.000	0.300	0.440	0.750
PANI/ITO plastic	TNT/ZnS NPs	9.5	2.650	4.100	1.600	0.275	0.400	0.550

It is apparent from Fig. 12 that using of bare TNT annealed at 550 ºC for 2h as a photoelectrode and PANI/ITO plastic as a counter electrode, the fabricated cell exhibited J_{sc} and V_{oc} and FF values of (1.4 mA cm^{-2}, 0.36 V and 0.52) respectively, resulting in a low power conversion efficiency of 0.3 %. The electrocatalytic activity of TNT electrode was very low which provides low current density. The optimized device of TNT/ZnS nanoparticles of ZnS pH value equal to 8.5 electrode exhibited the highest conversion efficiency of 0.75 % in the KI/I_2 electrolyte, which is higher than that of other photoelectrodes. Under illumination of simulated (80 mW cm^{-2}), the fabricated device showed J_{sc}, V_{oc} and FF values of (3.1 mA cm^{-2}, 0.44 V and 0.44), respectively. As mentioned previously, it can be concluded that the enhanced power conversion efficiency is caused by the insertion of ZnS nanoparticles layer on TNT, which leads to the enhancement of photo-electron harvesting efficiency of photoanode and relatively low resistivity.

Also, the performance of TNT/ZnS nanoparticles of ZnS pH values equal to 7.5 and 9.5 photoelectodes (η = 0.33%, J_{sc} = 1.8 mA cm^{-2}, V_{oc} = 0.38 V and FF = 0.48) and (η = 0.55 %, J_{sc} = 2.65 mA cm^{-2}, V_{oc} = 4.1 V and FF = 0.40) respectively. Because of a higher band gap of ZnS nanoparticles (3.75 eV) for pH 8.5 is caused by the quantum confinement effect, the excited electrons are confined inside TNT and the holes are localized in ZnS nanoparticles layer.

Fig. 12 illustrates the photocurrent enhancement of heat treated (after annealing) TNT of pure TNT and TNT/ZnS nanoparticles photoanodes for all devices. This enhancement resulted in the increasing of power conversion efficiency remarkably. This is attributed to the improvement of the film crystallinity after thermal annealing, which leads to the enhancement of power conversion efficiency performance of semiconductor heterostructures [13].

Conclusion

In summary, TiO_2 nanotube arrays/ZnS nanoparticles (TNT/ZnS NPs) photoanodes were successfully prepared *via* two deposition methods. TiO_2 nanotubes were first grown on titanium foil substrate by using anodization method followed by sequent chemical bath deposition method of ZnS nanoparticles onto TNT layer. It is demonstrated that ZnS nanoparticles deposited on the surface of TiO_2 nanotube films can be used as photoanodes in flexible DSSCs. The optimized device of TNT/ZnS nanoparticles photoelectrode of ZnS pH value equal to 8.5 in conjunction with KI/I_2 electrolyte and PANI on ITO plastic as a counter electrode, under illumination of simulated (80 mW cm^{-2}), exhibited the highest conversion efficiency of 0.75 %. The fabricated device showed J_{sc}, V_{oc} and FF values of (3.1 mA cm^{-2}, 0.44 V and 0.44) respectively. This proposed that the promising ZnS nanoparticles layer which deposited on TNT layer collects a large number of photo-injected electrons in the conduction band of photoanode and Ru-N719 dye reduce the recombination of photo-injected electrons with the redox electrolyte. Also, thermal annealing of TNT layer at 550 ºC and for 2 h leads to the enhancement of photoelectrochemical properties of TNT/ZnS nanoparticles photoanodes.

REFERENCES

1. J.H. Yang, C.W. Bark, K.H. Kim and H.W. Choi, *Materials*, **7**, 3522 (2014); https://doi.org/10.3390/ma7053522.
2. S.S. Kim, Y.C. Nah, Y.Y. Noh, J. Jo and D.Y. Kim, *Electrochim. Acta*, **51**, 3814 (2006); https://doi.org/10.1016/j.electacta.2005.10.047.
3. J. Yan and F. Zhou, *J. Mater. Chem.*, **21**, 9406 (2011); https://doi.org/10.1039/c1jm10274e.
4. F. Rezvani, E. Parvazian and S.A. Hosseini, *Bull. Mater. Sci.*, **39**, 1397 (2016); https://doi.org/10.1007/s12034-016-1278-8.
5. S.S. Rao, D. Punnoose, C.V. Tulasivarma, C.H.S.S. Pavan Kumar, C.V.V.M. Gopi, S.-K. Kim and H.-J. Kim, *Dalton Trans.*, **44**, 2447 (2015); https://doi.org/10.1039/C4DT03102D.
6. A.R. Yugis, R.F. Mansa and C.S. Sipaut, *IOP Conf. Series: Mater. Sci. Eng.*, **78**, 1 (2015); https://doi.org/10.1088/1757-899X/78/1/012003.
7. C. Wu, B. Chen, X. Zheng and S. Priya, *Sol. Energy Mater. Sol. Cells*, **157**, 438 (2016); https://doi.org/10.1016/j.solmat.2016.07.021.
8. M.S. Shinde, P.B. Ahirrao, I.J. Patil and R.S. Patil, *Indian J. Pure Appl. Phys.*, **49**, 765 (2011).
9. M. Reka Devi, B. Lawrence, N. Prithivikumaran and N. Jeyakumaran, *Int. J. Chemtech Res.*, **6**, 5400 (2014).
10. M. Mandal, D. Ghosh, S. Giri, I. Shakir and C.K. Das, *RSC Adv.*, **4**, 30832 (2014); https://doi.org/10.1039/C4RA03399J.
11. J. Vivekanandan, V. Ponnusamy, A. Mahudeswaran and P.S. Vijayanand, *Appl. Sci. Res.*, **3**, 147 (2011).
12. Z. Arifin, S. Soeparman, D. Widhiyanuriyawan and S. Suyitno, *Int. J. Photoenergy*, **Article ID 2704864** (2017); https://doi.org/10.1155/2017/2704864.
13. A.K. Ayal, Z. Zainal, H.-N. Lim, Z.A. Talib, Y.-C. Lim, S.-K. Chang and A.M. Holi, *Opt. Quantum Electron.*, **49**, 164 (2017); https://doi.org/10.1007/s11082-017-0985-8.